# Faraday Discussions

Accepted Manuscript


This manuscript will be presented and discussed at a forthcoming Faraday Discussion meeting. All delegates can contribute to the discussion which will be included in the final volume.

**Register now to attend!** Full details of all upcoming meetings: http://rsc.li/fd-upcoming-meetings

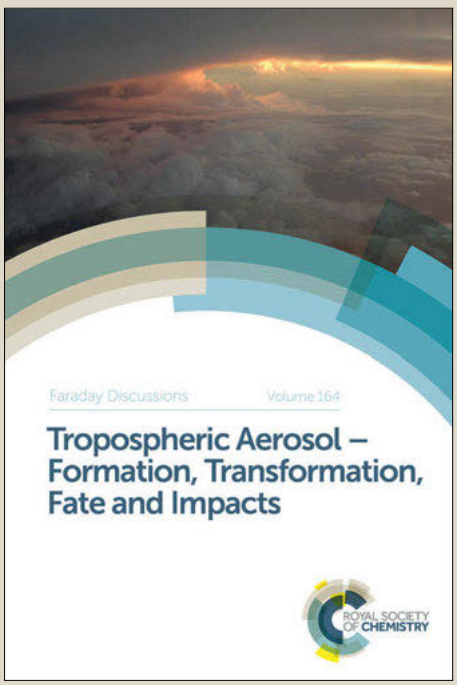


This is an *Accepted Manuscript*, which has been through the Royal Society of Chemistry peer review process and has been accepted for publication.

*Accepted Manuscripts* are published online shortly after acceptance, before technical editing, formatting and proof reading. Using this free service, authors can make their results available to the community, in citable form, before we publish the edited article. We will replace this *Accepted Manuscript* with the edited and formatted *Advance Article* as soon as it is available.

You can find more information about *Accepted Manuscripts* in the Information for Authors.

Please note that technical editing may introduce minor changes to the text and/or graphics, which may alter content. The journal's standard Terms & Conditions and the Ethical guidelines still apply. In no event shall the Royal Society of Chemistry be held responsible for any errors or omissions in this *Accepted Manuscript* or any consequences arising from the use of any information it contains.


ROYAL SOCIETY OF CHEMISTRY

www.rsc.org/faraday_d

PAPER Faraday Discussions www.rsc.org/xxxxxx | XXXXXXXX

# Glutamate biosensors based on diamond and graphene platforms

**Jingping Hu[a], Sirikarn Wisetsuwannaphum[b] and John S. Foord[b,*]**
**DOI: 10.1039/b000000x**

L-glutamate is one of the most important neurotransmitters in the mammalian central nervous system, playing a vital role in many physiological processes and implicated in several neurological disorders, for which monitoring of dynamic levels of extracellular glutamate in the living brain tissues may contribute to medical understanding and treatments. Electrochemical sensing of glutamate has been developed recently mainly using platinum, carbon fibre and carbon nanotube electrodes. In the present work, we explore the fabrication and properties of electrochemical glutamate sensors fabricated on doped chemical vapour deposition diamond electrodes and graphene nanoplatelet structures. The sensors incorporate platinum nanoparticles to catalyse the electroxidation of hydrogen peroxide, glutamate oxidase to oxidise glutamate, and a layer of poly-phenylenediamine to impart selectivity. The performance of the devices was compared to a similar sensor fabricated on glassy carbon. Both the diamond and the graphene sensor showed very competitive performance compared to the majority of existing electrochemical sensors. The graphene based sensor showed the best performance of the three investigated in terms of sensitivity, linear dynamic range and long term stability, whereas it was found that the diamond device showed the best limit of detection.

## 1 Introduction

The integration of biological tissues with electronic devices, to enable electrical stimulation of cells and electrical transduction of cellular signals, is at present an active topic in research to improve understanding of neuronal function[1, 2]. Whilst electrical stimulation and measurements of action potential can be achieved using microprobe electrodes, a more recent trend is the growth of cellular tissues at the interface with electrical devices such as microelectrode or open gated micro-transistor arrays to improve the quality of the data recorded and the study of cell assemblies[3-5]. A significant problem here is the design of cell-semiconductor interfaces which are sufficiently stable in physiological media. For example conventional Si chip technology undergoes drift and long term degradation because of the penetration of electrolyte ions into the transistor structure. The same problem is encountered with electrode and microelectrode assemblies for the electrochemical amperometric detection of the quantal release of neurotransmitters such as dopamine and norepinephrine. Here materials such as carbon fibre electrodes are often employed, but again degrade in the physiological media through oxidation and electrode fouling resulting in poor sensitivity and stability[6, 7].

An interesting advance to the problem of finding materials that are stable in physiological media for these applications, is the use of diamond grown by chemical

vapour deposition (CVD)[8, 9]. CVD diamond is now commercially readily available at modest price and when doped with boron becomes highly conductive displaying excellent electrochemical properties. In particular the high phase stability, resistance to fouling, low background capacitive current and wide range of operating potentials makes it ideal for use in hostile environments[10]. The material also lends itself to unique, highly sensitive transistor designs which overcome the materials issues inherent to Si chip technologies, for detection of cell electrical signals[3]. The use of a single platform material both for electrochemical and transistor-based electrical measurements offer unique possibilities for the future design of bioelectronic devices.

One step towards achieving this is the development of diamond-based electrode interfaces for the selective electrochemical detection of the neurotransmitter species of interest. In this context previous studies have focussed on the use of boron-doped diamond (BDD) for detection of species such as dopamine, norepinephrine, epinephrine, melatonin, catecholamine and adenosine *in vitro*[7, 11-14]. BDD electrodes have also been used to monitor serotonin *in vivo*, and demonstrated advantageous properties over carbon fibre electrodes including a very low background current and a high level of response stability even without the use of a protective polymer coating[12]. The application of BDD electrodes in the biosensing of glutamate has not been studied in any detail. Among the neurotransmitters detected by biosensors, L-glutamate is one of the most important in the mammalian central nervous system, playing a vital role in many physiological processes[15-17]. Its excess release is implicated in several neurological disorders, such as stroke, epileptic seizures and Parkinson's disease[18-20]. L-glutamate is most widely monitored *in vivo* by microdialysis methods, which are limited by poor spatial and slow time resolution[18]. An alternative approach, using electrochemical sensing methods, has been developed recently, using platinum[21, 22], glassy carbon[20, 22], and carbon nanotube electrodes[23], which provide an approach to an implantable amperometric sensor for continuous long term sensing, with a high spatial and temporal resolution.

Apart from the conventional solid carbon electrodes such as graphite and glassy carbon, over the past decade research in electrochemistry has focused increasingly on the use of dispersed forms of carbon of which perhaps the most important has been carbon nanotubes because of their high surface area, ease of chemical functionalisation, suitability for enzyme immobilisation, and enhanced electrochemical activity through edge-plane like defects[24]. Difficulties in purification however can give rise to undesired properties[25]. Graphene platelets are another form of dispersed carbon material[26], which is now evoking high interest within electrochemistry. Attractive characteristics include high surface area (2630 $m^2/g$ twice as much as that of SWCNTs)[27], low cost, ease of processing[28], unique thermal and mechanical properties and high electrical conductivity. Graphene has therefore become an attractive and promising novel nanomaterial in various applications. For example, in fuel cell development, a graphene-based electrode was shown to outperform CNT-based ones in terms of electrocatalytic activity[29] and provided better macroscopic scale conductivity in biosensing application[30]. The material has been widely employed for bioanalytical applications such as in detection of glucose[31, 32], dopamine[33], NADH[34, 35], $H_2O_2$[36] and glutamate based on field effect transistor configuration using CVD grown graphene[37].

The glutamate biosensor is based on the oxidation of glutamate in the presence of glutamate oxidase.

$$Glutamate + O_2 + H_2O \rightarrow \alpha - ketoglutarate + NH_3 + H_2O_2 \quad (1)$$

The $H_2O_2$ produced in this reaction is electroactive at electrodes such as Pt so providing a route to infer the concentration of glutamate, although it is inactive at many typical carbon-based electrodes which are often used, necessitating addition of various electrocatalytic material such as Pt nanoparticles[21], hydrous iridium oxide[38], Prussian blue[39] or peroxidase enzymes including horseradish peroxidase[40], cytochrome c peroxidase[41], or catalase enzyme[42], or heme peptide such as hemoglobin[43].

In the present work we thus investigate the extent to which electrochemical detection of glutamate can be achieved using conductive diamond and graphene as the electrode materials, activated with Pt electrocatalytic species that can catalyse the oxidisation of hydrogen peroxide[21, 22]. However, even in the presence of platinum electrocatalyst, a high positive potential (>0.5 V vs Ag/AgCl) is expected for the oxidation of $H_2O_2$. At this potential, some endogenous electroactive species, such as ascorbate, urate, dopamine, acetaminophen, and catecholamines, are also oxidized. This undermines the selectivity of the biosensor[39] and requires screening strategies to eliminate the problem. The polymer poly-phenylenediamine is used in this regard in the present work.

The performance of BDD and graphene based glutamate sensors formed in this way is explored in this article. In particular the sensitivity, selectivity and stability of the biosensors are characterised and compared with those based on the more established conventional glassy carbon based electrodes which we fabricate using similar methods.

## 2 Experimental

### 2.1 Reagents and solutions

The enzyme glutamate oxidase (GluOx, EC 1.4.3.11) from Streptomyces sp. was supplied from Sigma Aldrich, as was L-Glutamic acid (Glu, >99.5%), m-phenylenediamine (PPD, >99%), glutaraldehyde (GA, 50% in water), hydrogen peroxide (50 wt% in water), L-ascorbic acid (AA), Uric acid (UA, Sigma) and 4-Acetamidophenol (AP, Aldrich). Dihydrogen hexachloroplatinate (IV) hexahydrate ($H_2PtCl_6{\cdot}6H_2O$, 99.9%) was obtained from Alfa Aesar. $NaBH_4$ (Fluka), Poly(diallyldimethylammonium chloride) solution 20 wt% in water (Aldrich), sodium chloride (Fluka) were in analytical grade and used as supplied. Graphene oxide 0.5 wt% in water with a thickness of around 3 nm and 550 nm in size was purchased from Angstron Materials.

The supporting electrolyte used was phosphate buffered saline solution (PBS) consisting of 0.137 M NaCl (Aldrich, >99%), 0.0027 M KCl (Fluka, >99.5%), 0.01 M $Na_2HPO_4$ (Sigma-Aldrich, >99%) and 0.002 M $KH_2PO_4$ (Sigma, >99%), and adjusted to pH 7.4 with sodium hydroxide (Fisher, 98.7%). All solutions were prepared with distilled Milli-Q water (>18 MΩcm).

### 2.2 Instrumentation

Polished smooth (average roughness Ra<30 nm) BDD and glassy carbon discs of 3 mm diameter and 0.5 mm thickness obtained from Element Six Ltd (Ascot, UK) were used as rotating disk electrodes (RDE). Experiments were conducted at 20 ± 2 $^{o}$C using a CHI900B electrochemical workstation in a standard three-electrode setup

with a Ag/AgCl reference electrode against which all potentials quoted in this paper are measured with respect to, and a platinum counter electrode. Prior to use, the BDD electrode was cleaned by potential cycling between -1.6 and 2.5 V in 0.5 M sulphuric acid for 20 cycles to remove contaminants from the surface. The glassy carbon electrode was cleaned by polishing with alumina powder to a mirror finish and ultrasonicating in ethanol and water respectively. The electrode was stored in PBS in a fridge (4 $^{o}$C) after GluOx functionalization.

TEM images were taken using JEOL JEM-2000FX equipment with an accelerating voltage of 200 kV. Tapping-mode AFM was conducted with a Digital Instruments Multimode Nanoscope Scanning Probe Microscope (Veeco Metrology Group). The XPS measurements were conducted using a hemispherical analyser spectrometer with Al $K_{\alpha}$ radiation (hν=1486.6eV). Zeta potential was measured using a Zetasizer NanoZS (Malvern Instruments) at 25°C and all the samples were diluted to 0.1mg/mL.

## 3 Results and Discussions

### 3.1 Preparation and Characterisation of Platinum nanoparticle decorated BDD electrodes and graphene nanoplatelets

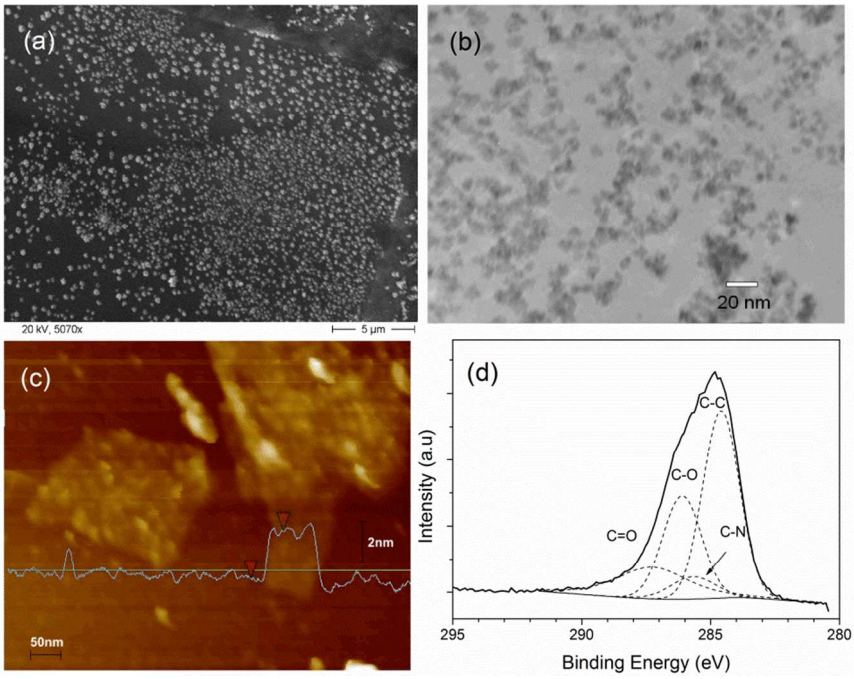


**Fig. 1** SEM image of Pt modified diamond electrode showing the presence of Pt clusters on the diamond surface (a), TEM (b) and AFM (c) images of 50wt% Pt on PDDA graphene nanoplatelets showing uniform distribution of Pt nanoparticles on graphene surface and the thickness of graphene sheet respectively and XPS spectrum of carbon 1s of the same sample (d)

The first step in sensor fabrication was the preparation of electrode materials decorated with Pt nanoparticles. Electrodeposition is a well-established approach which creates adherent metal nanoparticles on diamond electrodes, whereas coatings

of pre-formed nanoparticles tend to be easily lost from the very inert diamond surface. Platinum particles were therefore electrodeposited on the BDD electrode from a solution of 2 mM $H_2PtCl_6$ dissolved in 0.5 M $H_2SO_4$, using a fixed electrode potential of -0.2 V for 10 minutes as we have described previously [44]. The exact procedure used leads to the formation of electrode surfaces decorated with stable, roughly 150±30 nm diameter porous Pt clusters with a coverage of $3\times10^8$ particles $cm^{-2}$, as illustrated by the secondary electron microscope image in Fig. 1(a). The total Pt electroactive area is around 13 times bigger than the physical area of the electrode, for which details are given elsewhere [44].

In contrast a wet chemical approach could instead be used to prepare Pt functionalised graphene, which has the ability to form more dispersed materials. To achieve this, graphene oxide was first functionalised with Poly(diallyldimethyl -ammonium chloride) (PDDA) by mixing 50 mg of graphene oxide with 0.5 wt% of PDDA and 1 wt% of NaCl in aqueous solution which was then ultrasonicated to obtain a stable suspension. Graphene oxide carries a negative charge, so the purpose of the PDDA which is a cationic polyelectrolyte is to change this to a positive charge, thus attracting the $[PtCl_6]^{2-}$ to the graphene surface. This was confirmed with zeta potential measurements; graphene oxide possesses negative zeta potential of -26.7 mV and this switched to positive zeta potential of 63.7 mV after functionalisation with PDDA confirming the successful adsorption of PDDA on to the surface of graphene oxide. Due to this, PDDA functionalised graphene oxide becomes more susceptible for reaction with the $[PtCl_6]^{2-}$ complex and the amount of Pt on the graphene can be easily tuned by simply adjusting the quantity of the added platinum precursor. The mixture was filtered and washed several times to remove excess PDDA, and dried in air for 24 hours. Then 5mg of PDDA functionalised graphene oxide was dispersed in 10 mL of water by ultrasonication followed by adding 10.5 mg of $H_2PtCl_6$ and 50 mM HCl and was ultrasonicated for 15 minutes. 0.5 mL of 200 mM $NaBH_4$ (in large excess) in 200 mM NaOH was added drop wise to this mixture under vigorous stirring for 1 hour. The resulting solution was filtered and washed several times with water followed by drying in air overnight. This sample is referred to as 50% loading, which corresponds to the percentage weight in the Pt-graphene composite if complete reaction between the added graphene and Pt occurred. Similarly 15% and 70% loadings were also prepared. Electrode fabrication was then carried out by drop coating 5 µL of 1 mg/mL suspension of Pt-graphene onto the glassy carbon electrode.

The morphology of platinum graphene nanoplatelets composites (Pt-GNPs) produced from simultaneous reduction of hexachloro platinate (IV) complex and PDDA functionalized graphene oxide was elucidated by transmission electron microscopy in Fig. 1(b). The average Pt particle size was estimated to be around 8 nm with a narrow range of size distribution. Fig. 1(c) shows the typical AFM image of Pt-GNPs on Si substrate. The thickness of reduced graphene oxide sheet was found to be 2.4 nm on average corresponding to a few monolayers of graphene and is comparable to the thickness of PDDA functionalised graphene nanoplatelets reported elsewhere[45].

To further characterize the surface chemical composition of the Pt-GNPs hybrid, XPS analysis was carried out. In the survey scan (data not shown), there are three main peaks observed at around 72 eV, 285 eV, and 531 eV in all Pt-graphene nanosheets samples, which correspond to Pt 4f, C 1s and O 1s respectively and one small peak at 402 eV due to N 1s from PDDA. The higher resolution spectra provide

closer investigation of the chemical states on the surface of C 1s in Fig 1(d). The peak at binding energy of 284.5 eV can be assigned to graphitic C-C bond, while those at higher binding energies correspond to C-OH (286.2 eV) and C=O (287.2 eV) bonds [46]. Additionally, a small peak observed at 285.7 eV is suggested which is consistent with the presence of C-N bonds from PDDA.

The relative surface composition of Pt to C in Pt-GNPs was estimated from XPS data with an atomic sensitivity factor of Pt 4f of 4.4 [47] to be 5.5% for Pt deposited on GNPs, giving rise to 2.4 μg loading of Pt for 5 μg Pt-GNPs used for the sensor fabrication. This corresponds to 50% loading of Pt precursor to the reaction mixture in the synthesis step. The electrochemical active surface area of the Pt was estimated by the charge associated with the oxidation of adsorbed hydrogen[48] and found to be 2.6 $cm^2$. By contrast the Pt-BDD electrode showed a twofold higher Pt loading of 5.1 μg but a lower surface area of 0.98 $cm^2$. This trend is qualitatively consistent with the larger particle size of the Pt-BDD electrode.

### 3.2 Comparison of Pt-BDD and Pt-GNPs platform for detection of hydrogen peroxide and glutamate

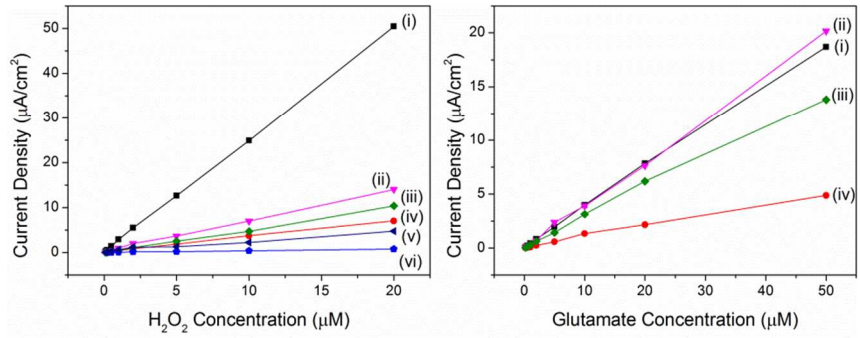


**Fig. 2** Linear plot of current density response (a) against concentration of $H_2O_2$ and (b) glutamate measured at different electrodes; (i) Pt modified boron-doped diamond, (ii) 50wt%, (iii) 70wt%, (iv) 15wt% Pt loading on graphene nanosheets, (v) graphene nanosheets and (vi) Pt nanoparticles as controlled experiments

As briefly explained in the introduction, the mechanism of the oxidation of L-glutamate catalysed by L-glutamate oxidase enzyme can be represented by the following two-step process.

$$L-glutamate + H_2O + GluOx/FAD \rightarrow \alpha-ketoglutarate + NH_3 + GluOx/FADH_2 \quad (2)$$

$$GluOx\ /\ FADH_2\ + O_2 \rightarrow GluOx/FAD + H_2O_2 \quad (3)$$

The first step is the deamination process catalysed by glutamate oxidase enzyme with the cofactor flavin adenine dinucleotide (FAD) acting as a redox centre. Upon the uptake of the oxygen co-substrate in the second step, hydrogen peroxide is produced as a by-product. The production of $H_2O_2$ can then be directly detected at the electrode by the electrocatalytic oxidation as shown below.

$$H_2O_2 \rightarrow O_2 + 2H^+ + 2e^- \quad (4)$$

Measurement of $H_2O_2$ oxidation activity was therefore compared on the 2 types of electrode. The as-prepared platinum decorated diamond sensor (Pt-BDD) shows a reproducible oxidisation peak at about 0.5 V in the anodic scans of cyclic

voltammograms measured in stirred $H_2O_2$ electrolyte. The chronoamperometric response of the electrode was thus measured at 0.5 V in PBS for varying hydrogen peroxide concentrations by addition of small amounts of 10 mM $H_2O_2$ solution using a RDE electrode rotated at 3000 rpm to accelerate the mixing.

A linear plot of current density against concentration of $H_2O_2$ was observed at least up to 20 μM as presented in Fig. 2(a). Similar experiments for the Pt-GNPs electrode were also carried out for which data is also presented in Fig. 2(a). The Pt-BDD electrode exhibited the highest sensitivity of 2.5 μA $\mu M^{-1}$ $cm^{-2}$ while the 50wt% Pt-GNPs despite being the highest amongst the Pt-GNPs samples showed a sensitivity of 0.69 μA $\mu M^{-1}$ $cm^{-2}$. Although lowering the amount of Pt added to the graphene to 15% reduced the response to $H_2O_2$ (curve (iv) in figure 2(a)) as expected it was found that increasing the amount of Pt had little effect, as can be seen in figure 2(a) where the 70% loaded sample produced even a smaller sensitivity than the 50% loading. It is not clear what differences between the differing electrodes are responsible for these differing responses. In comparing the performances of the differing sensors however, it should be borne in mind that the Pt-BDD electrode is significantly more responsive to $H_2O_2$ than is the Pt-GNPs modified electrode.

For control experiments, Pt-PDDA and GNPs-PDDA electrodes were also tested (traces (v) and (vi) in Fig. 2(a)). However the $H_2O_2$ sensitivity of both falls well below that of Pt-GNPs confirming that both graphene itself and also Pt nanoparticles coated with PDDA are relatively inactive towards $H_2O_2$ oxidation as expected[32, 49, 50].

### 3.3 Detection of glutamate at low concentrations

The enzyme immobilisation step was carried out by drop evaporation of glutamate oxidase, using around 1 mg glutamate oxidase in 5 μL of PBS solution [22], on the Pt-BDD electrode and the 50wt%Pt-GNPs. It was then stabilised on the surface by exposure to glutaraldehyde (GA) vapour for 10 minutes, which has been shown to efficiently immobilise glutamate oxidase on surfaces through cross-linking of amino groups [51]. The response of the electrodes to glutamate was then tested at a potential of 0.5 V for well-stirred PBS solutions containing differing concentrations of glutamate. The concentration of glutamate is around 10 μM in the brain extracellular fluid [52] and around 20 μM in serum and cerebrospinal fluids [53], so concentrations in this range are of primary interest for practical applications.

The Pt-BDD/GluOx sensor shows a linear response at low glutamate concentrations (0.2 to 50 μM) as shown in Fig. 2(b), with a sensitivity of 370 nA $\mu M^{-1}$ $cm^{-2}$, which leads to a detection limit (signal:noise (s/n) = 3) of 220 nM for the 3 mm diameter diamond electrode used, given the typical background noise level of 2 nA in our measurement system. Limits of detection for most electrochemical glutamate sensors are typically in the range 200 nM- 2μM so the performance of the diamond sensor is very competitive in this regard [22, 23, 54-57]. In comparison, the 50wt%Pt-GNPs/GluOx sensor shows a slightly higher response of 400 nA $\mu M^{-1}$ $cm^{-2}$ for the same linear range measured with a detection limit of 320 nM (s/n=3) due to higher background noise. It is interesting to note out that the glutamate sensitivity of Pt-BDD, despite possessing much higher hydrogen peroxide sensitivity, becomes similar to the glutamate response of Pt-GNPs. By contrast, for the graphene platform, the trend between different platinum loadings follows that observed for $H_2O_2$ response as seen in Fig. 2(b). This suggests a higher activity or more efficient enzyme immobilisation on the graphene surface as compared to the diamond surface

in the fabrication methodology employed.

### 3.4 Selectivity and effects of modifying the diamond sensor with poly-phenylenediamine

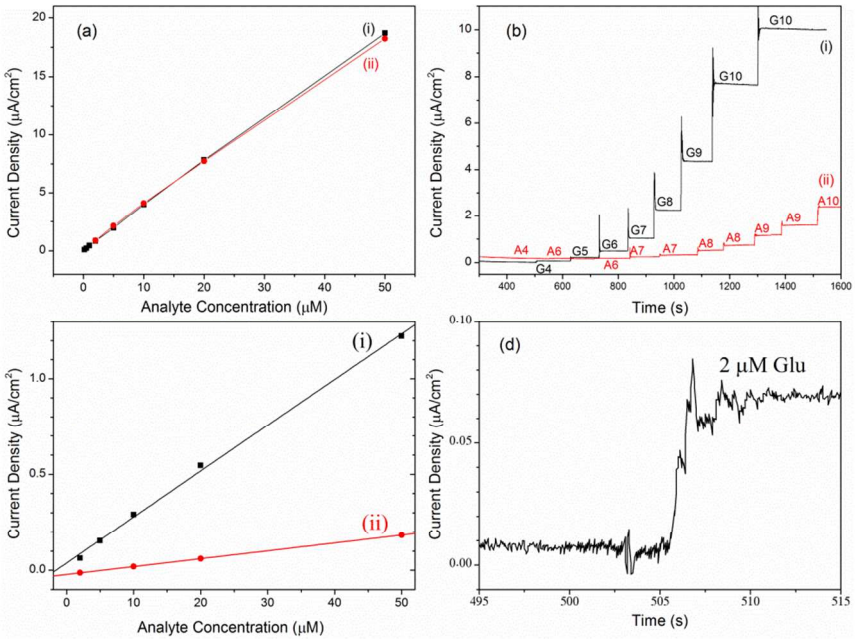


**Fig. 3** (a) Calibration curve for the diamond glutamate sensor without a PPD layer for the response to glutamate (i) and ascorbic acid (ii) in a stirred PBS solution. (b) Amperometric response curve of the glutamate sensor with a PPD layer at 0.5 V upon successive injection of (i) glutamate or (ii) ascorbic acid solution in a stirred PBS buffer: 2, 5, 10, 20, 50, 100, 200 μM for G4 to G10 or A4 to A10 respectively. (c) the corresponding calibration plot and (d) background signal noise level of the amperometric response in (b)

The operation of bio-sensors is susceptible to interference by endogenous electroactive species, especially ascorbic acid[22, 52] which is normally present at significant concentrations and is easily oxidised. Interference of ascorbic acid, unsurprisingly, is therefore also observed in our diamond glutamate sensor, as shown in Fig. 3(a), which shows equal sensitivity to glutamate and ascorbic acid. A typical method to eliminate the interference of endogenous species is the use of a permselective membrane such as Poly-phenylenediamine (PPD) to inhibit the diffusion of larger molecules such as ascorbic acid, while still allowing the diffusion of small molecules such as $H_2O_2$ to the electrode surface [58]. PPD was thus deposited as a barrier layer to enhance the selectivity. PPD polymerisation onto the electrode was conducted at 0.7 V for 1 minute in 100 mM phenylenediamine solution prepared in PBS using the Pt-decorated diamond electrode before functionalisation with the GluOx. The glutamate sensor was then characterized after at least 5 days storage in PBS at 4 $^{o}$C in a fridge to achieve stable operating characteristics as discussed in the next section before being subject to systematic measurements.

The diamond sensor with a PPD layer exhibits a much improved selectivity to glutamate than to ascorbic acid, as shown in Fig. 3 (b) and (c), although unsurprisingly the sensitivity is reduced by over a factor of 10. The diamond sensor

incorporating the PPD layer shows a sensitivity to ascorbic acid of 4 nAμM$^{-1}$cm$^{-2}$, 6 times smaller than the sensitivity to glutamate (24 nAμM$^{-1}$cm$^{-2}$) as shown in the linear plot of current density against analyte concentration in Fig. 3(c). The linear range is still up to 50 μM, but the glutamate detection limit is increased to 350 nM (s/n=3) as a result of the change in sensitivity as illustrated in Fig. 3(d).

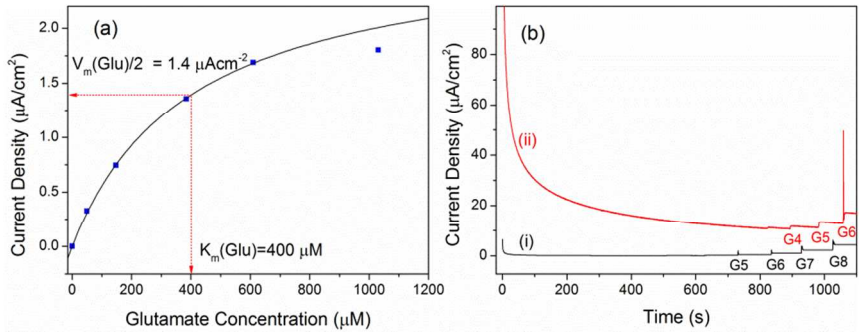


**Fig. 4** (a) Calibration plot for diamond glutamate sensor with a PPD layer at high glutamate concentration. The solid line is the best curve fit to the Michaelis-Menten model (b) Amperometric response for (i) BDD based and (ii) glassy carbon based glutamate biosensor at 0.5 V upon successive addition of glutamate to stirred PBS buffer: 5, 10, 20, 50, 100 μM for G4 to G8 respectively

At high glutamate concentrations, the sensor current becomes non-linear as expected and shows characteristics of the Michaelis-Menten kinetics mechanism, as depicted in Fig. 4(a). The enzyme catalysed reaction can be described by the Michaelis-Menten equation,

$$I_{ss} = V_m[S]/(K_m + [S]) \quad (5)$$

where $I_{ss}$ is the steady state current at a given reagent concentration [S], $V_m$ is the maximum current at enzyme saturation, and $K_m$ is the Michaelis-Menten constant, corresponding to the reagent concentration when $I_{ss}$ is equal to half of maximum current ($V_m$).

A higher $V_m$ value and a lower $K_m$ value are desired for the best sensitivity. The data suggests a $K_m$ value for the diamond glutamate sensor of around 400 μM, greater than the value for the free enzyme which is 200 μM, but encouragingly lies to the lower end of the reported range of $K_m$ values for surface bound glutamate oxidase (250 – 2800 μM) [17, 52]. The variation of $K_m$ value is influenced by several aspects, such as steric and electrostatic hindrance by neighbouring GluOx enzymes [17]. The $V_m$ value depends especially on the loading of GluOx enzyme, and the sensor fabricated here shows a $V_m$ value of 2.8 μA cm$^{-2}$. As observed elsewhere, the PPD layer has little influence on $K_m$ but reduces $V_m$ [17]. It is expected that a thicker PPD layer could improve the selectivity further, but this is achieved at the cost of sensitivity. The work here therefore incorporates the PPD loading at this level, which represents a compromise between optimal sensitivity and selectivity.

Since differing fabrication procedures in different laboratories can produce varying performance levels making comparisons difficult, an identical sensor was fabricated, but using a glassy carbon electrode rather than diamond to compare the influence of the two substrates. Although qualitatively similar performance levels were noted, significant differences were also found. For both sensors some

stabilisation when immersed in background PBS electrolyte is needed to achieve a sensitive analytical performance. Comparisons are made in Fig. 4(b) showing chronoamperometric response curves. The diamond sensor exhibits a small background current density when it is activated in blank solution and rapidly reaches a steady state, enabling fast monitoring of glutamate concentration changes. This must stem in part from the inert nature of the diamond electrode and the low interfacial capacitance, which is known to yield low electrochemical background current densities for this material [59]. In contrast the glassy carbon based sensor shows a large background signal when it is first activated in blank solution so a long incubation time is required before measurements can commence. Even after equilibration the background current is much larger than for the diamond sensor. Because of the varying and large background current, the detection limit was about 2.4 μM (s/n=3), significantly higher than reported above for the diamond device, and comparable to what is observed for glutamate sensors based on carbon fiber [60] and glassy carbon [20, 22].

Since changes in the background signal are often the limiting issue in controlling the sensitivity of electrochemical measurements in this type of application, rather than signal:electrical noise ratios [7, 12], it is useful to consider the signal:background (S/B ratio) of an electrochemical sensor system. After the background current has stabilised, the glassy carbon based glutamate sensor exhibits an S/B ratio of 0.02 $\mu M^{-1}$, similar to the value observed previously for a similar sensor [22]. In comparison the same work shows a ratio of around 0.55 $\mu M^{-1}$ for Pt, Au and Pd based glutamate biosensors. In contrast, an S/B ratio of 2.8 $\mu M^{-1}$ is found for the diamond based glutamate sensor, around 140 times higher than that for the glassy carbon device. This stems solely from the low and stable background current seen for the diamond sensor.

### 3.5 Selectivity and effects of modifying the graphene sensor with poly-phenylenediamine

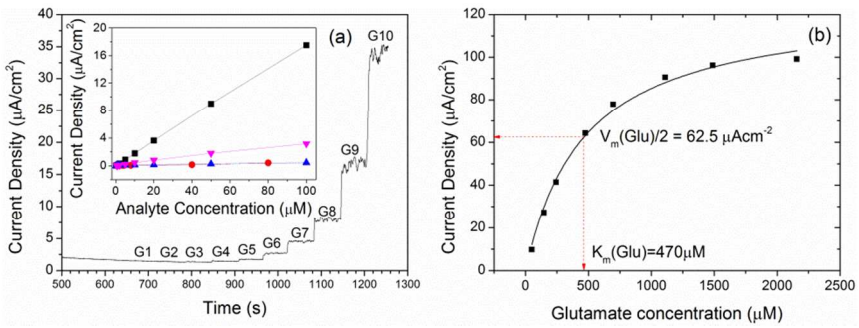


**Fig.5** (a) Amperometric response of 50% Pt-GNPs in stirred PBS buffer at 0.5V with successive additions of increasing concentration of glutamate: 0.1, 0.2, 0.5, 1, 2, 5, 10, 20, 50, 100 μM for G1 to G10 respectively with the inset showing the linear plot of current density against concentrations of glutamate (■) in comparison to commonly found interfering species in physiological conditions; uric acid (●), ascorbic acid (▲) and 4-acetamiophen (▼). (b) Michaelis-Menten plot of current density against concentration of glutamate at 0.5 V by 50% Pt-GNPs.

The glutamate biosensor based on Pt-GNPs was similarly modified with PPD to improve selectivity The performance of the GC/Pt-GNPs/GluOx/PPD electrode in glutamate sensing was investigated also by amperometric sensing at 0.5 V with

successive injections of increasing glutamate concentration into thoroughly stirred PBS solution as shown in Fig. 5(a). The electrode exhibited a good linear response range up to 100 μM with a high sensitivity of 174 $nA\mu M^{-1} cm^{-2}$ , reflecting a smaller loss of sensitivity with addition of PPD than was observed for the diamond device. Good reproducibility was again seen with less than 10% response variation from sensor to sensor. The detection limit, LOD (s/n=3) was found to be 0.75 μM roughly two times higher than for diamond.

The fitted Michaelis-Menten curve of the GC/Pt-GNPs/GluOx/PPD electrode plotted in Fig. 5(b) revealed that $K_m$ = 470 μM which is comparable to that observed for diamond above and the maximum reaction rate, $V_m$ is 125.0 $\mu Acm^{-2}$ much higher than for the diamond electrode since the loss of activity due to addition of PPD is less.

As previously noted for the diamond sensor, several ubiquitous electrochemically active species in brain fluid may interfere with the sensor affecting the detection of glutamate. This nonetheless was minimised by addition of PPD as before. This permselective membrane provides cation-selective permeability[61] and hence successfully eliminated the interference from ascorbic acid as well as uric acid and the 4-acetamidophenol as shown as calibration plots in the inset of Fig. 5(a).

### 3.6 Long term stability

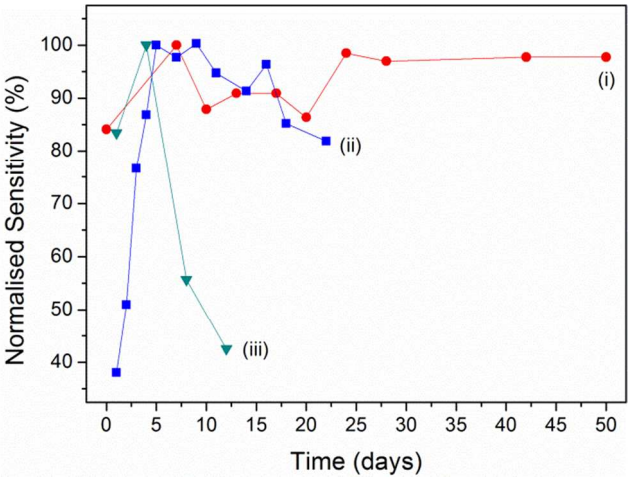


**Fig.6** Normalised sensitivity of (i) glutamate sensors based on Pt-GNPs (ii) Pt-BDD and (iii) Pt-glassy carbon as a function of storage time from fabrication.

The reproducibility and stability of the fabricated diamond and graphene glutamate sensors were examined, and compared with that of glassy carbon based sensor, as shown in Fig. 6. All three sensors show an increasing sensitivity in the initial days after fabrication, which may be attributed to opening of membrane channels in the PPD layer[62], the swelling of PPD membrane[63, 64] and conformational relaxation of the glutamate oxidase enzyme[65] when the electrode was stored in buffer solutions. After the relaxation period, the glassy carbon based sensor shows faster decay to less than 50% of its best performance in a week, as seen for similar devices such as SWCNT and Os-gel-HRP modified glassy carbon sensor for glutamate or NADH[51, 66]. Frequent measurements and high accumulative concentration of glutamate also have shown adverse effect on the stability of glutamate biosensors, probably due to

denaturation of enzyme by local decrease of pH value as a result of hydrogen peroxide oxidation[63]. Despite the high glutamate concentrations used in the stability test, the diamond based glutamate sensors still demonstrated rather stable performance with less than 20% decay in the next three weeks. The graphene based sensor on the other hand maintained around 90% of its highest sensitivity over a long period of 7 weeks. The good long term stability of diamond and graphene based glutamate sensor is attributed to good biocompatibility and the excellent electrochemical stability of the two substrates[67].

**Table 1** Comparison of glutamate sensing performance by sensors developed in our laboratory, which emphasizes the largely enhanced sensitivity and linearity range by Pt-graphene hybrid electrode

| | GC/Pt-GNPs/GluOx/PPD | GC/Pt/PPD/GluOx | BDD/Pt/PPD/GluOx |
|---|---|---|---|
| Pt loading/μg | 2.4 | 5.1 | 5.1 |
| LoD/μM | 0.75 | 2.4 | 0.35 |
| Linearity/μM | 0.2-100 | 0.5-50 | 0.5-50 |
| Sensitivity/ $nA\mu M^{-1}cm^{-2}$ | 174 | 91 | 24 |
| Time response/s | 4 | 5 | 4 |
| $V_m/\mu Mcm^{-2}$ | 125 | - | 2.8 |
| $K_m/\mu M$ | 470 | - | 400 |

## 4. Concluding remarks

Electrochemical glutamate biosensors for bioelectronic applications have been demonstrated using boron doped diamond and graphene for the first time. In terms of limit of detection, stability and sensitivity, the devices exhibit comparable or in many cases significantly improved levels of performance compared to similar electrochemical devices produced on other platforms in the past [23, 55, 57, 68, 69].

Since similar sensor fabrication approaches were used to produce devices on three different substrates, the suitability of the characteristics of these substrates with regard to the fabrication procedures used can be judged. Relevant parameters and overall sensor performance, for the devices fabricated, are summarised in Table 1. The mass of Pt was calculated for the diamond and glassy carbon electrodes from the electrolysis charge, whereas for the graphene electrodes from mass added during drop coating using the Pt content as deduced from XPS. The GC/Pt-GNPs/GluOx/PPD electrode structure exhibited superior overall performance particularly in terms of enhanced sensitivity and wide linear range, with the diamond platform showing poor sensitivity, largely because more activity seemed to be lost here when PPD was deposited in comparison to the other electrode materials. However the BDD/Pt/PPD/GluOx sensor on the other hand shows a more desirable detection limit due to very low background and electrical noise. All the sensors exhibited fast time response making them suitable for real-time measurement. Significant differences in stability were also observed. When freshly immersed in PBS buffer, the glassy carbon electrode required long stabilisation times (Fig. 4(b)) and in the stability testing rapid degradation were observed over a timescale of the order of 7 days. In contrast, the diamond sensor showed good stability for the three weeks it was tested for, whist the graphene device showed good stability over a period of seven weeks. Overall the present work illustrates how diamond and

graphene materials can be used successfully for glutamate sensing.

## Acknowledgement

We would like to acknowledge the financial support from Engineering and Physical Sciences Research Council (EPSRC) in the UK with grant no. EP/F025513/1. S. Wisetsuwannaphum also would like to thank the Royal Thai government for funding the PhD studentship.

## References

[a]*Huazhong University of Science and Technology, School of Environmental Science and Engineering, Wuhan, P.R. China 430074 E-mail: hujp@hust.edu.cn ; Tel: +86-27-87792207*
[b]*Chemistry Research Laboratory, Department of Chemistry, University of Oxford, Mansfield Rd, Oxford, OX1 3TA, UK. Fax: +44 1865 275410; Tel: +44 1865 275967; E-mail: john.foord@chem.ox.ac.uk*
**contact for correspondence*

1. G. C. Albert, C. M. Cook, F. S. Prato and A. W. Thomas, *Neurosci. Biobehav. Rev.*, 2009, **33**, 1042-1060.
2. A. L. Benabid, B. Wallace, J. Mitrofanis, C. Xia, B. Piallat, V. Fraix, A. Batir, P. Krack, P. Pollak and F. Berger, *C. R. Biol.*, 2005, **328**, 177-186.
3. M. Dankerl, S. Eick, B. Hofmann, M. Hauf, S. Ingebrandt, A. Offenhausser, M. Stutzmann and J. A. Garrido, *Adv. Funct. Mater.*, 2009, **19**, 2915-2923.
4. P. Fromherz, A. Offenhausser, T. Vetter and J. Weis, *Science*, 1991, **252**, 1290-1293.
5. S. Ingebrandt, C. K. Yeung, M. Krause and A. Offenhausser, *Biosens. Bioelectron.*, 2001, **16**, 565-570.
6. J. Park, V. Quaiserova-Mocko, B. A. Patel, M. Novotny, A. H. Liu, X. C. Bian, J. J. Galligan and G. M. Swain, *Analyst*, 2008, **133**, 17-24.
7. J. Park, Y. Show, V. Quaiserova, J. J. Galligan, G. D. Fink and G. M. Swain, *J. Electroanal. Chem.*, 2005, **583**, 56-68.
8. J. H. T. Luong, K. B. Male and J. D. Glennon, *Analyst*, 2009, **134**, 1965-1979.
9. L. Tang, C. Tsai, W. W. Gerberich, L. Kruckeberg and D. R. Kania, *Biomaterials*, 1995, **16**, 483-488.
10. R. G. Compton, J. S. Foord and F. Marken, *Electroanal*, 2003, **15**, 1349-1363.
11. J. Park, J. J. Galligan, G. D. Fink and G. M. Swain, *Anal. Chem.*, 2006, **78**, 6756-6764.
12. B. A. Patel, X. H. Bian, V. Quaiserova-Mocko, J. J. Galligan and G. M. Swain, *Analyst*, 2007, **132**, 41-47.
13. E. Popa, H. Notsu, T. Miwa, D. A. Tryk and A. Fujishima, *Electrochem. Solid-State Lett.*, 1999, **2**, 49-51.
14. S. T. Xie, G. Shafer, C. G. Wilson and H. B. Martin, *Diamond Relat. Mater.*, 2006, **15**, 225-228.
15. T. Bruhn, T. Christensen and N. H. Diemer, *J. Neurosci. Methods*, 1995, **59**, 169-174.
16. A. A. Karyakin, E. E. Karyakina and L. Gorton, *Anal. Chem.*, 2000, **72**, 1720-1723.
17. C. P. McMahon, G. Rocchitta, P. A. Serra, S. M. Kirwan, J. P. Lowry and R. D. O'Neill, *Analyst*, 2006, **131**, 68-72.
18. J. J. Burmeister, F. Pomerleau, M. Palmer, B. K. Day, P. Huettl and G. A. Gerhardt, *J. Neurosci. Methods*, 2002, **119**, 163-171.
19. J. Castillo, A. Blochl, S. Dennison, W. Schuhmann and E. Csoregi, *Biosens. Bioelectron.*, 2005, **20**, 2116-2119.

20. R. Maalouf, H. Chebib, Y. Saikali, O. Vittori, M. Sigaud and N. Jaffrezic-Renault, *Biosens. Bioelectron.*, 2007, **22**, 2682-2688.
21. J. H. Han, H. Boo, S. Park and T. D. Chung, *Electrochim. Acta*, 2006, **52**, 1788-1791.
22. R. D. O'Neill, S. C. Chang, J. P. Lowry and C. J. McNeil, *Biosens. Bioelectron.*, 2004, **19**, 1521-1528.
23. K. B. Male, S. Hrapovic and J. H. T. Luong, *Analyst*, 2007, **132**, 1254-1261.
24. C. E. Banks, T. J. Davies, G. G. Wildgoose and R. G. Compton, *Chemical Communications*, 2005, 829-841.
25. I. Dumitrescu, P. R. Unwin and J. V. Macpherson, *Chemical Communications*, 2009, 6886-6901.
26. K. S. Novoselov, A. K. Geim, S. V. Morozov, D. Jiang, Y. Zhang, S. V. Dubonos, I. V. Grigorieva and A. A. Firsov, *Science*, 2004, **306**, 666-669.
27. A. K. Geim and K. S. Novoselov, *Nat Mater*, 2007, **6**, 183-191.
28. M. Segal, *Nature Nanotechnology*, 2009, **4**, 611-613.
29. R. I. Jafri, T. Arockiados, N. Rajalakshmi and S. Ramaprabhu, *J. Electrochem. Soc.*, 2010, **157**, B874-B879.
30. S. Alwarappan, A. Erdem, C. Liu and C. Z. Li, *J. Phys. Chem. C*, 2009, **113**, 8853-8857.
31. C. S. Shan, H. F. Yang, J. F. Song, D. X. Han, A. Ivaska and L. Niu, *Anal. Chem.*, 2009, **81**, 2378-2382.
32. X. H. Kang, J. Wang, H. Wu, I. A. Aksay, J. Liu and Y. H. Lin, *Biosens. Bioelectron.*, 2009, **25**, 901-905.
33. N. G. Shang, P. Papakonstantinou, M. McMullan, M. Chu, A. Stamboulis, A. Potenza, S. S. Dhesi and H. Marchetto, *Adv. Funct. Mater.*, 2008, **18**, 3506-3514.
34. L. H. Tang, Y. Wang, Y. M. Li, H. B. Feng, J. Lu and J. H. Li, *Adv. Funct. Mater.*, 2009, **19**, 2782-2789.
35. H. Liu, J. Gao, M. Q. Xue, N. Zhu, M. N. Zhang and T. B. Cao, *Langmuir*, 2009, **25**, 12006-12010.
36. M. Zhou, Y. M. Zhai and S. J. Dong, *Anal. Chem.*, 2009, **81**, 5603-5613.
37. Y. X. Huang, X. C. Dong, Y. M. Shi, C. M. Li, L. J. Li and P. Chen, *Nanoscale*, 2010, **2**, 1485-1488.
38. C. Terashima, T. N. Rao, B. V. Sarada, N. Spataru and A. Fujishima, *J. Electroanal. Chem.*, 2003, **544**, 65-74.
39. F. Ricci and G. Palleschi, *Biosens. Bioelectron.*, 2005, **21**, 389-407.
40. Y. J. Teng, S. H. Zuo and M. B. Lan, *Biosens. Bioelectron.*, 2009, **24**, 1353-1357.
41. L. Zhang, *Biosens. Bioelectron.*, 2008, **23**, 1610-1615.
42. K. B. O'Brien, S. J. Killoran, R. D. O'Neill and J. P. Lowry, *Biosens. Bioelectron.*, 2007, **22**, 2994-3000.
43. N. Q. Jia, Q. Lian, Z. Y. Wang and H. B. Shen, *Sensors Actuators B: Chem.*, 2009, **137**, 230-234.
44. J. Hu, X. Lu and J. S. Foord, *Electrochem. Commun.*, 2010, **12**, 676–679.
45. K. Liu, J. Zhang, G. Yang, C. Wang and J.-J. Zhu, *Electrochem. Commun.*, 2010, **12**, 402-405.
46. S. Stankovich, R. D. Piner, X. Q. Chen, N. Q. Wu, S. T. Nguyen and R. S. Ruoff, *J. Mater. Chem.*, 2006, **16**, 155-158.
47. e. D. B. a. M. P. S. C. D. Wagner, *Practical Surface Analysis*, 2nd edn., J. Wiley and Sons, 1990.
48. A. Pozio, M. De Francesco, A. Cemmi, F. Cardellini and L. Giorgi, *J. Power Sources*, 2002, **105**, 13-19.

49. Y. Y. Shao, S. Zhang, C. M. Wang, Z. M. Nie, J. Liu, Y. Wang and Y. H. Lin, *J. Power Sources*, 2010, **195**, 4600-4605.
50. W. Qin and X. Li, *J. Phys. Chem. C*, 2010, **114**, 19009-19015.
51. Z. M. Liu, O. Niwa, T. Horiuchi, R. Kurita and K. Torimitsu, *Biosens. Bioelectron.*, 1999, **14**, 631-638.
52. M. R. Ryan, J. P. Lowry and R. D. ONeill, *Analyst*, 1997, **122**, 1419-1424.
53. R. L. Villarta, G. Palleschi, A. Suleiman and G. G. Guilbault, *Electroanal*, 1992, **4**, 27-31.
54. M. Ammam and J. Fransaer, *Biosens. Bioelectron.*, 2010, **25**, 1597-1602.
55. N. Hamdi, J. J. Wang, E. Walker, N. T. Maidment and H. G. Monbouquette, *J. Electroanal. Chem.*, 2006, **591**, 33-40.
56. V. M. Tolosa, K. M. Wassum, N. T. Maidment and H. G. Monbouquette, *Biosens. Bioelectron.*, 2013, **42**, 256-260.
57. T. T. C. Tseng, J. Yao and W.-C. Chan, *Biochem. Eng. J.*, 2013, **78**, 146-153.
58. L. T. Cai and H. Y. Chen, *Sensors Actuators B: Chem.*, 1999, **55**, 14-18.
59. M. Wei, Y. L. Zhou, J. F. Zhi, D. G. Fu, Y. Einaga, A. Fujishima, X. M. Wang and Z. Z. Gu, *Electroanal*, 2008, **20**, 137-143.
60. O. M. Schuvailo, S. Gaspar, A. P. Soldatkin and E. Csoregi, *Electroanal*, 2007, **19**, 71-78.
61. J. M. Elliott, L. M. Cabuche and P. N. Bartlett, *Anal. Chem.*, 2001, **73**, 2855-2861.
62. E. Ekinci, S. T. Ogunc and A. E. Karagozler, *J. Appl. Polym. Sci.*, 1998, **68**, 145-152.
63. K. S. Chang, W. L. Hsu, H. Y. Chen, C. K. Chang and C. Y. Chen, *Anal. Chim. Acta*, 2003, **481**, 199-208.
64. X. N. Zhang and G. A. Rechnitz, *Electroanal*, 1994, **6**, 361-367.
65. S. A. M. Marzouk, S. S. Ashraf and K. A. Al Tayyari, *Anal. Chem.*, 2006, **79**, 1668-1674.
66. L. Meng, P. Wu, G. X. Chen, C. X. Cai, Y. M. Sun and Z. H. Yuan, *Biosens. Bioelectron.*, 2009, **24**, 1751-1756.
67. H. L. Fan, L. L. Wang, K. K. Zhao, N. Li, Z. J. Shi, Z. G. Ge and Z. X. Jin, *Biomacromolecules*, 2010, **11**, 2345-2351.
68. M. Zhang, C. Mullens and W. Gorski, *Electrochim. Acta*, 2006, **51**, 4528-4532.
69. S. Chakraborty and C. R. Raj, *J. Electroanal. Chem.*, 2007, **609**, 155-162.